Imaging hard – inside the skeleton

Timothy G. Bromage, Santiago Gomez, Alan Boyde

Vertebrate hard tissue biologists study the surface and below-surface microanatomical features and compositional characteristics of bones and teeth of the skeleton (fish scales also deposit calcium phosphate and calcium carbonate into their structure, and we include them among the tissues we study). The variability in bone and tooth histology rivals that of all other organ systems, making it an ideal tissue for understanding the development, function, and physiology of organisms. What is more, in deference to soft tissues, bones and teeth survive as fossils, permitting all that we can know from the skeleton about an organism living today to be extrapolated to animals living millions of years ago.

By and large, hard tissues are formed by cells that secrete an organic matrix, which then mineralises. But in some cases they may be made from soft tissues such as cartilage or ligament that subsequently mineralise. While it may appear counterintuitive, the development of a bone often also requires bone-removing cells to allow the re-sizing and re-shaping of a bone during development. These bone-removing cells also assist in the maintenance of bone throughout life by a process of removal of small packets of tissue followed by the replacement of tissue by forming cells.

Bones and teeth are hard because of the largely calcium and phosphate mineral deposited into them. Regarding this point, the first mistake most hard tissue biologists make is to give their research specimens to a routine histology laboratory that commences to demineralise their specimens and make them soft! This permits the laboratory to make paraffin embedded thin sections using specialist knives. There are a handful of us in the world that can honestly say, "we are *hard* tissue biologists", and who have the opinion that to throw away more than half of a bone or tooth's mass is not the best starting point for obtaining a complete understanding of the nature of the tissue. This is all the more important in light of microscopy techniques we employ and describe below to visualise the histocomposition of hard tissues. However, if we wished to image the collagen fabric of say, a bone, in greater detail, we may decalcify the embedded mineralised section, leaving only the collagen for providing morphological contrast.

Microscopy

A variety of microscopy technologies and techniques are employed on either intact unprepared bone and tooth tissues, or those infiltrated with and embedded into plastic and cut with any one of a number of precision saws. In our laboratories we employ stereo zoom and compound light microscopy, white light and laser confocal microscopy, real time 3D microscopy, and scanning electron microscopy.

Bright-field microscopy

Bright-field is the simplest yet most versatile form of microscopy. Specimens imaged by bright-field microscopy - usually histological sections - are illuminated by transmitted light from below in an upright microscope (or from above in an inverted microscope). The specimen must provide all of the potential contrast. Contrast mechanisms vary, and those typically used in our laboratories include manipulating the obliquity of the illuminating light by opening-closing the back aperture, or by employing darkfield, phase, and differential interference contrast techniques.

Applying histological stains to sections imaged by bright-field microscopy also provides useful contrast; in our laboratories, Stevenel's blue and Toluidine blue are commonly used, which, on bone, produce coloured optical density variability relating to mineralisation density differences. We do not stain tissues prior to embedding, but rather stain the surfaces of our thick (e.g., 100 µm) sections. These stains penetrate 5-10 µm below the surface, and when imaged above an opaque white diffusing plate, present an image formed almost exclusively from the stained thickness layer; this image is equivalent to a stained 5-10 µm thick decalcified paraffin-embedded section.

Polarising microscopy

Birefringent materials - like hydoxy apatite with negative intrinsic birefringence - or stacked structures like collagen molecules, microfibrils and fibrils, with water in between which give positive form birefringence, generate orientation-dependent contrast in polarising microscopy. Most polarising microscopes in the world employ a linear polariser filter on the illumination side of the specimen and a "crossed" linear analyser filter on the imaging side of the specimen. Increasing brightness in the image is associated with the degree to which the birefringent components are in the plane of the section. However, the crossed linear polarising filter arrangement renders an artefactual darkness along two axes furthest from the maximum transmission axes of the two filters. Brightness in images derived from linear polarising microscopes is thus not easily quantifiable nor always fully interpretable because of this artefact.

The linear polarising problem is eliminated by steering photons into a helical trajectory rather than a plane one, and under this condition, the light is polarised in all 360 degree rotational positions; this is called circularly polarised light (CPL) (Boyde et al., 1984; Bromage et al., 2003b). This is accomplished by placing a complementary quarter wave filter between the specimen and each linear polarising filter. Image brightness under CPL conditions is a true signal representative of the orientation of the collagen in bone, dentine, and cementum. The contrast generated provides insight on the development and function of the tissue.

Further contrast enhancing techniques associated with polarising microscopy can be obtained by introducing compensator and/or bandpass cut-off filters or dichroic mirrors.

Confocal microscopy

Confocal microscopes belong to the family of scanning imaging technologies. A small aperture or slit translated across the field of view transmits both the illuminating beam and the emitted or reflected light returning from the object, which, for reasons of the geometry of the system, returns exclusively from the plane of focus of the objective lens. A single pinhole scanned across the entire field of view takes a bit of time, and thus the image must be built up. However, by using many thousands of pinholes on a spinning Nipkow disc, the holes interlace in space and integrate in time to produce a real time confocal image of the entire field of view when spun at video rate.

Laser confocal microscopes are used almost exclusively for exciting fluorophores and detecting fluorescence with high spatial resolution in the Z axis. White light confocal microscopes imaging in air present themselves as superior surface reflection instruments for metrology. In addition to this, by using an immersion objective lens or by placing a glass coverslip with a medium onto the specimen when using an objective in air, specular reflections are eliminated and the illuminating beam is allowed to penetrate deep to the surface. The consequence of these conditions for both laser and white light confocal microscopes begs the most interesting question; what if we drive the plane of focus of the objective lens below the surface of our opaque material? The result is an image composed of only that light emitted or reflected from the Z region occupied by the depth of focus of the objective lens.

There is a lot of material in the world we would like to image. Most of it is not in the lab, nor is there any evidence to suggest that it will come to the lab any time soon. Thus, we have to accept that if we wish to acquire knowledge about it at a microscopic scale, we have to go where the material is, and we must take our microscopes with us. A big advantage of white light Nipkow disc confocal microscopes is that they do not require a lot of hardware, such as a laser source or power supply. We thought that a portable confocal scanning optical microscope (PCSOM) would satisfy if it was packed into two pieces of approved check-in luggage for air travel, if it was robust to whatever it is that happens after check in, and if it was adaptable to "field" conditions and operating on 110 or 220 V. A number of images below were taken with this system and we briefly describe it here.

We used a PCSOM based on the Nipkow disk technique, described in detail by Petran and Hadravsky (1966) and first commercialised in the early 1980s; applications to hard tissue biology are available in Boyde (1983), and the history and various technical achievements in confocal microscopy are summarised in Boyde (1995). We utilise a "single-sided" Nipkow disk design in which the illumination and detection pinholes are the same (Kino, 1995). We configured our PCSOM to contend with the variety of conditions encountered at museums around the

world (Bromage, 2003a). An interesting feature of the design of our confocal module was the solution applied to suppress internal non-image-related reflections. Linear polarising light filters and a single quarter wave plate are employed for this purpose. The unintended benefit of this strategy was that the light returned from below-surface birefringent materials such as the collagen in bone tissue forms a reflected circularly polarised light confocal image.

Real time 3D microscopy

Our laboratories include several compound microscopes used for visualising real time 3D through the eyepiece objectives (Greenberg and Boyde, 1997). One of these microscopes uses linearly polarised multiple oblique transmission illumination, in which, by means of isolating left and right eyepiece objectives with their corresponding linear polarising analysers, enables a left and right eye stereoscopic view. The reflected light version of the real time 3D microscopy works by splitting vertically the image of the objective aperture and diverting it to its respective left and right eyepiece objectives. Both microscopes achieve real time viewing employing a single objective lens.

The high numerical aperture objective lenses used on these microscopes enabled us to perform through focus imaging to produce image stacks to be manipulated by software that combines all in-focus content into 3D image reconstructions.

Scanning electron microscopy

The scanning electron microscope (SEM), as the name implies, belongs to the family of scanning imaging technologies. An electron beam is formed from the heating of a source, such as a tungsten wire or solid state crystal, which is typically accelerated to 1-25 kV. The beam is focused by electromagnetic lenses and then scanned in a raster in X across the field of view, line by line in Y, at all times in register with the display monitor to acquire an image. A variety of events occurs at the focused on point, which detectors are designed to distinguish. Secondary electron (SE) detectors are used to observe SEs having lower energies than the incoming beam and that are ejected in large numbers from atoms encountered by the beam on the surface. Their propagation is substantially determined by topographic variability, and thus SE-SEM is a superior method for visualising morphologies on surfaces.

Backscattered electron (BSE) detectors are sensitive to electron energies at and slightly less than that of the incoming beam. Upon encountering the surface, many of the beam's electrons scatter back and away from the surface in proportion to the compositional density of the material. This BSE-SEM atomic number contrast is sensitive to topography and working distance, thus it is typically performed on polished surfaces plane to the incident beam. BSE-SEM is a valuable imaging method for visualising and measuring mineralisation density variability. Depending upon the accelerating voltage of the beam, some BSEs will backscatter from a small volume beneath the incident beam, but as this is typically less than one cubic micron, this imaging modality provides density-dependent images at higher resolution than any other method. BSE-SEM imaging is also used for visualising the iodine vapor infiltration of soft tissue microanatomy (Boyde et al., 2014). In addition, because some BSEs experience inelastic behavior and lose a small amount of energy before backscattering, specific energy windows may be opened to reveal additional contrast mechanisms.

Another area of research in which we have had success is that related to the production of high resolution replicas of bone and tooth surfaces with silicone impression materials commonly employed in dental practice (Bromage, 1987). These materials are used to make a negative impression of a surface, and combined with the production of positive replicas made from epoxy, render sub-micrometer surface resolution. Epoxy replicas of bone and tooth surfaces are taken back to the laboratory and examined by the SEM. Such studies have yielded a wealth of information about skeletal development and life history.

Bone tissues

3D human bone tissue

Figure 1 shows a 3D image of a blood vessel channel (top and centre of image) taken by conventional transmission compound microscopy, that is contained within layers of human bone tissue called lamellae and imaged by circularly polarised light. 24 2D images taken 3 microns apart were acquired in a through focus series, comprising a digital 24-image data set. This 72 µm thick portion of bone is part of a larger bone cross section taken from the middle of a human thighbone. Using 3D reconstruction software, the data set was virtually reconstructed into the 3D tissue block (Figure 2). Various colour schemes were applied to the lamellae depending upon the orientation of their collagen, and areas of surrounding lamellae (bottom and left) were rendered transparent to enable a look at internal features (Figure 3).

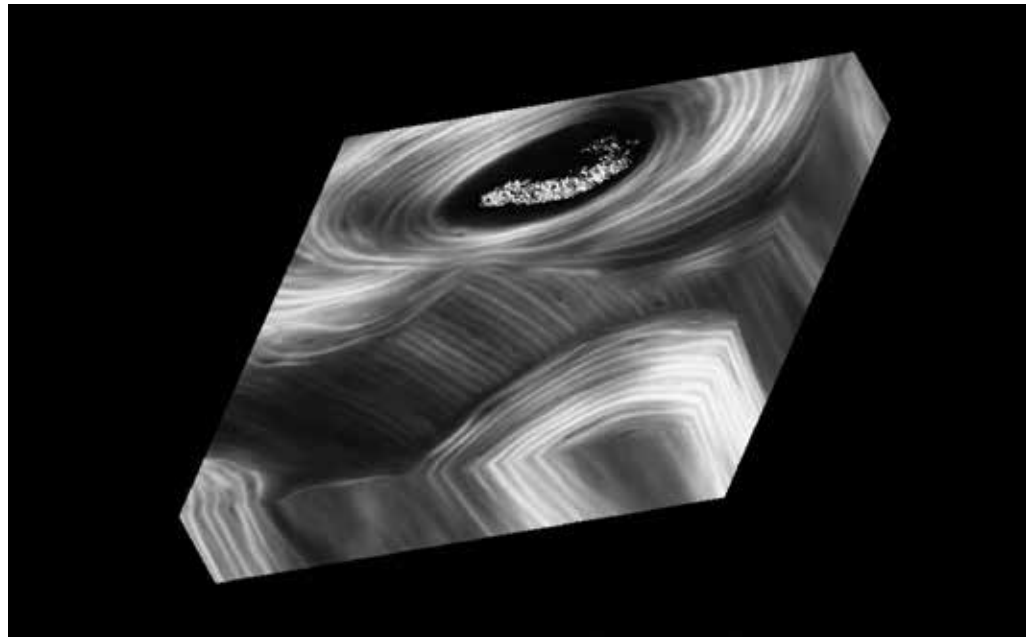

Figure 1. 3D grey-level image of a blood vessel with it's surrounding bone layers (lamellae). Width of slab 1.5 mm.

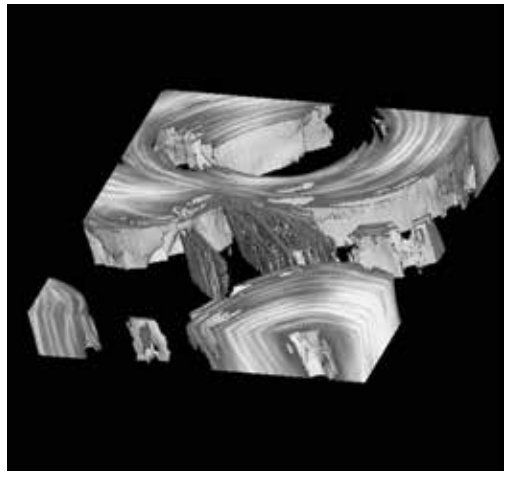

Figure 2. 3D Bone, grey-level images showing isolated areas of interest, while outer areas of surrounding lamellae are rendered transparent. Width of slab 1.5 mm.

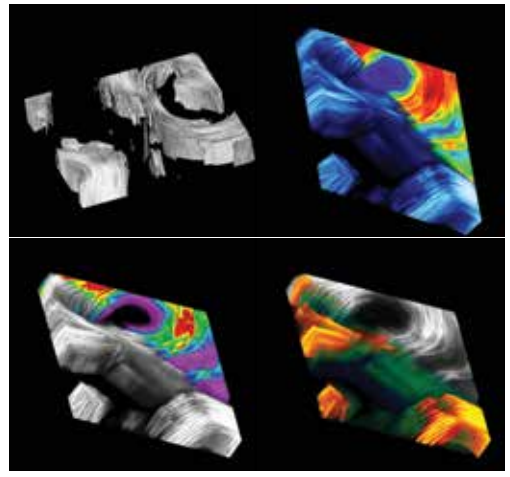

Figure 3. Rendering the 3D image by varying the colour spectrum as well as the degree of opacity and transparency enables novel features within bone to become apparent. Width of slab 1.5 mm.

Atapuerca cave attack

Bones from fossil bearing deposits at Atapuerca's Sima de los Huesos in northern Spain, which are approximately 0.4 million years old, have been subject to bacterial attack during fossilisation. This has eliminated much of the internal microanatomy, but left the external macroanatomy in perfect condition. In order to visualise the internal structures of these bones we used our PCSOM to obtain images of the collagen autofluorescence in ultraviolet light. Figure 4 shows a 3D image of the bacterial attack, the colours depicting damage at various levels from bottom (blue) to top (red). In 2D the colours appear mixed up because of the degree and nature of the attack, but by using diffraction grating glasses, the 3D is reconstructed. The bacterial attack also occurs in roughly circular "plaques" of damage (Figure 5).

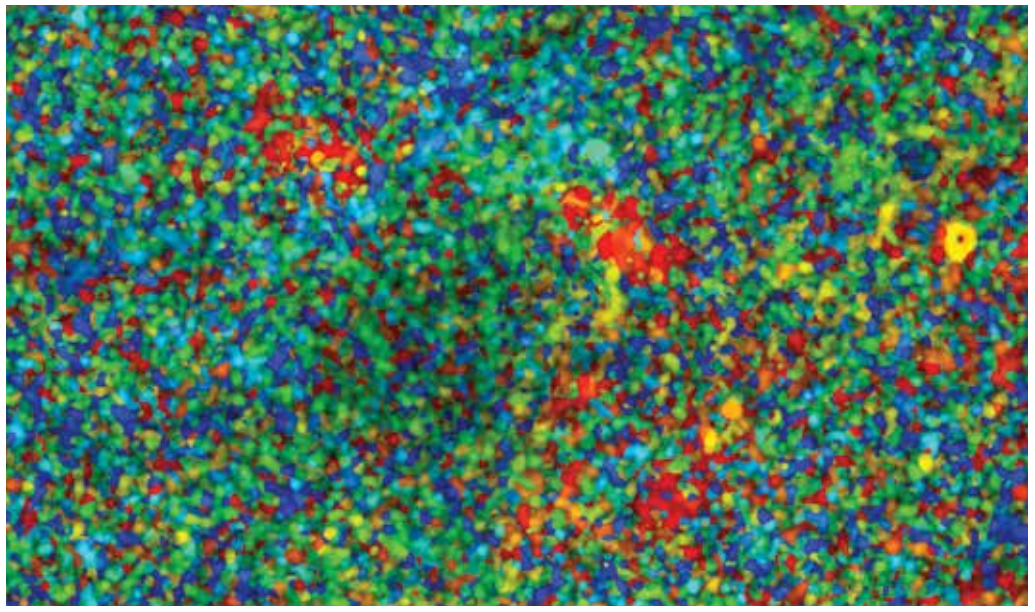

Figure 4. 3D image of cave bear bone produced by PCSOM. Field width 700 µm.

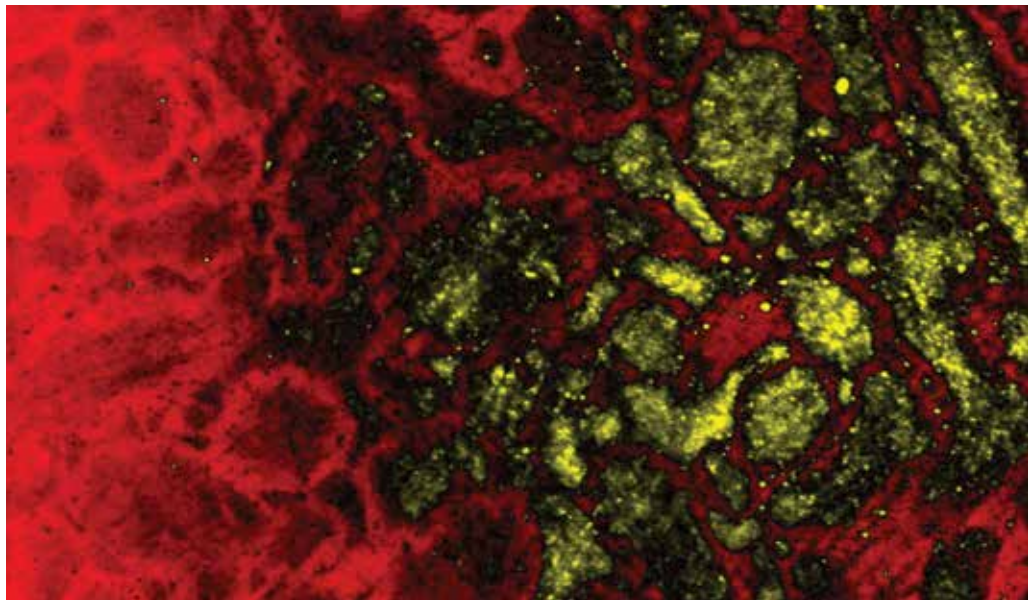

Figure 5. Image of cave bear tooth root (dentine) microanatomy produced by PCSOM. Field width 700 µm.

Grotte du Taï

A bone "plaque" from Grotte du Taï, France, ca. 10,000 BC, contains a continuous serpentine set of engraved marks interpreted to have been made daily for a period of more than three years. These marks have been imaged by direct view incident light 3D microscopy, in which a through series of images was reconstructed to provide a surface (Figure 6), a red-green anaglyph (Figure 7), and a colour depth map (Figure 8). The Taï plaque raised significant interdisciplinary psychological and neuropsychological discussions. Study of the plaque has concentrated on reconstructing the behaviour of the engraver by examining the marks in 3D. The marks change their characteristics every 28 days, thus they represent earliest lunar timekeeping from the beginning of the Neolithic period.

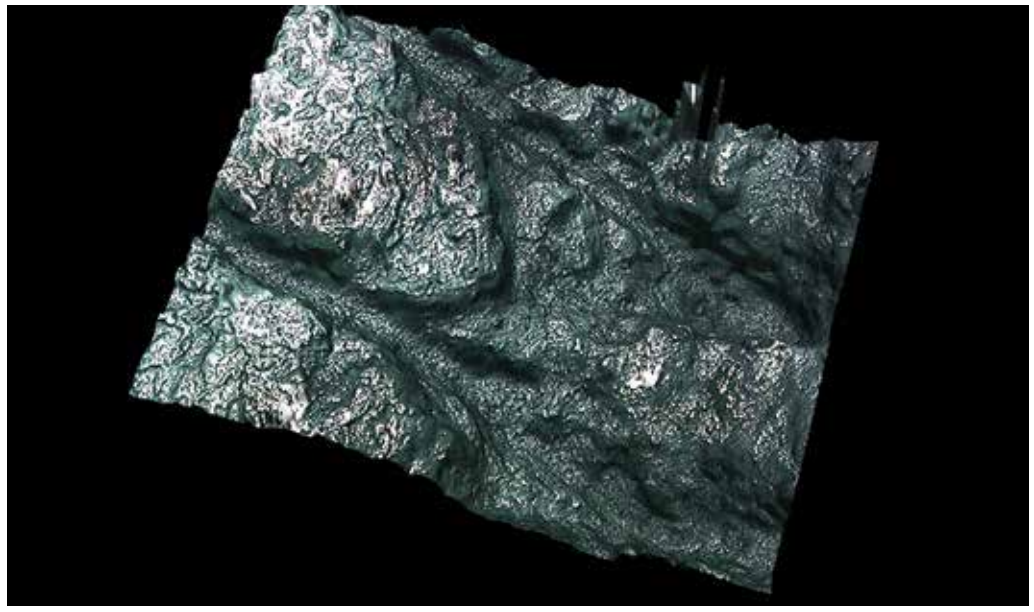

Figure 6. A through series, or image stack, of two marks were compiled into a pseudo 3D model. Field width of reconstruction 1.5 mm.

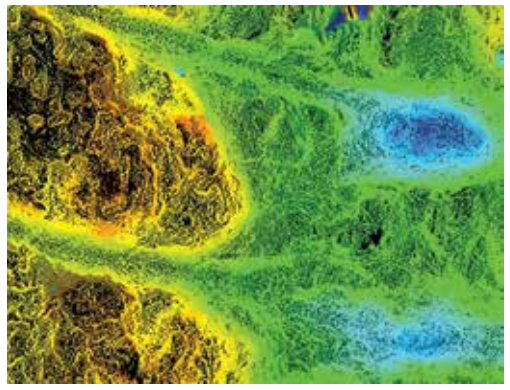

Figure 7. Depth characteristics are rendered as a colour-coded map. From deepest to highest, the colours grade from dark blue, through greens at intermediate heights, and yellows, reds, and brown at the highest points on the tool. Field width 1.5 mm.

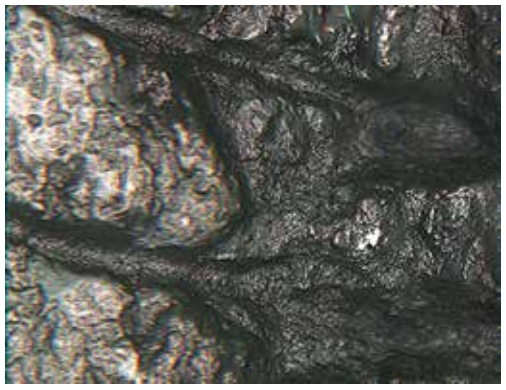

Figure 8. The image stack is reconfigured as left and right views that are here colour coded as green and red respectively. This image, referred to as an anaglyph, can be viewed in 3D with the aid of red-green glasses. Field width 1.5 mm.

Embryo

Using transmitted and incident light on a stereo zoom microscope, we imaged the 16.5-day old embryo of a "knockout mouse" in which the gene coding for an enzyme responsible for cell division has been inactivated (Yeh et al., 2007) Genetic manipulation of the mouse revealed the roles that genes play in the differentiation and development of the skeleton. The embryo here was cleaned of soft tissues and stained to reveal cartilage (blue) and mineralised bone (red) for study (Figure 9) (the white background has been rendered black). Research on gene knockout mice is contributing vital information concerning normal and abnormal development, which can then be used in future work on the evolution of skeletal structure or therapies for clinically relevant skeletal disorders and other diseases in humans.

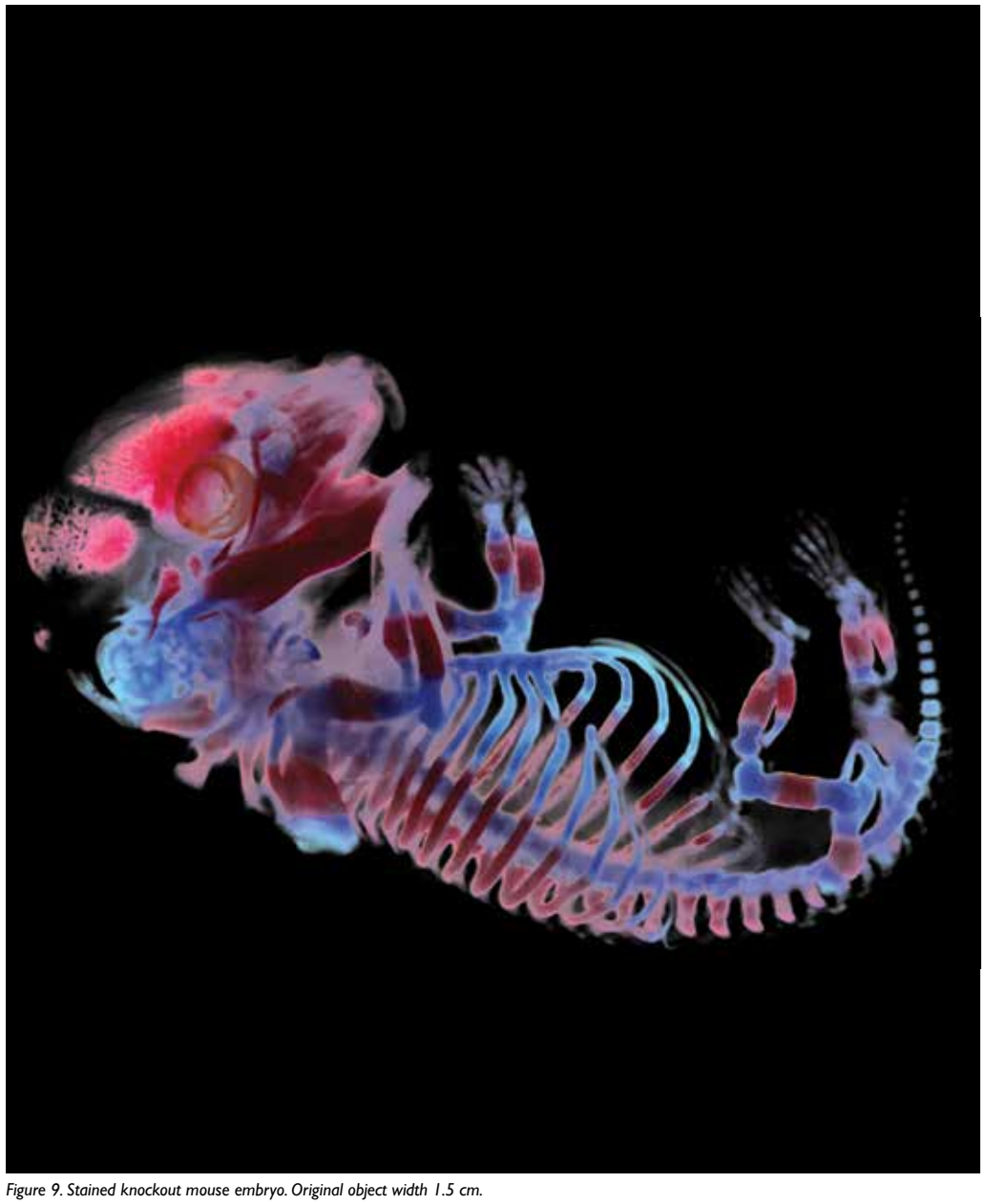

Figure 9. Stained knockout mouse embryo. Original object width 1.5 cm.

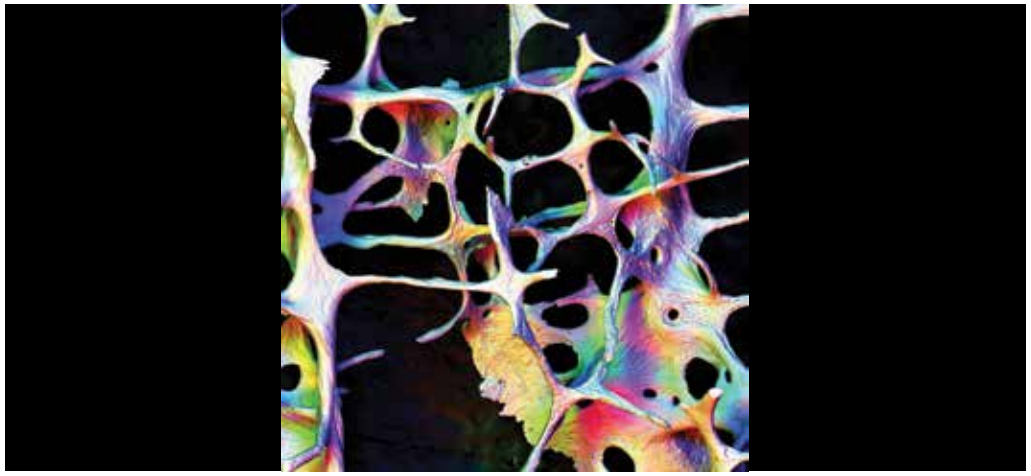

Figure 10. Human trabecular bone by BSE-SEM. Field width 4.45 mm.

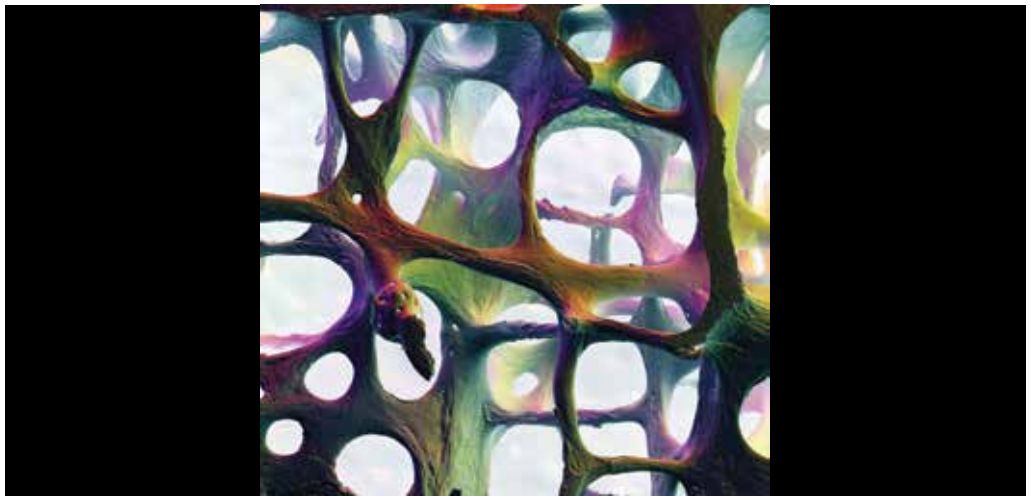

Figure 11. Human trabecular bone by BSE-SEM. Field width 4.0 mm.

Human trabecular bone

Figure 10 shows the spongy (trabecular) bone from the lumbar vertebra of an 89-year-old female as observed by BSE-SEM. Colour hue shows the spatial orientation (direction in which it is facing) and colour intensity shows the slope of the surface. 11 levels (in-focus planes at consecutive depths) of 250 microns each were recorded separately to provide an image in good focus at all depths. This image, and the technique employed to produce it, allows a better discrimination of bone surface activity than has been achieved before. In this elderly female, the beams of bone making up the inner architecture of the vertebra are significantly thinned compared to pre-menopausal woman. The novel imaging methods portrayed here affords a new perspective on osteoporosis.

Figure 11 shows an image produced by SEM of vertical slice of cancellous bone from a fourth lumbar vertebral body from an elderly female. This composite figure was made from 36 BSE-SEM images; 12 focus levels at 250 micron Z separation. At each focus level, four images were recorded with each of the separate backscattered electron detector sectors. Three of these images were combined by assigning the grey level image to one of three RGB colour channels. Rendering the composite image in negative contrast gives the pleasing back-lit effect

All in focus images make it possible to see structural detail over all surfaces over a large depth range.

Emu

Figure 12 shows an image of 100 µm thick bone section from the femur (thigh) of an Emu, a large flightless bird from Australia. The image was acquired by multiple oblique 3D microscopy, in which a through series of images was reconstructed to provide an all-in-focus image. The image has been colour coded according to depth in the bone. Dark blue-green structures illustrate a deep plexus of vascular canals, coursing more or less from left to right, that run circumferentially around the bone. Light blue striae represent surface marks at the bottom of the section left by the sawing of the bone and the yellow striae are similar marks on the very top surface of the section.

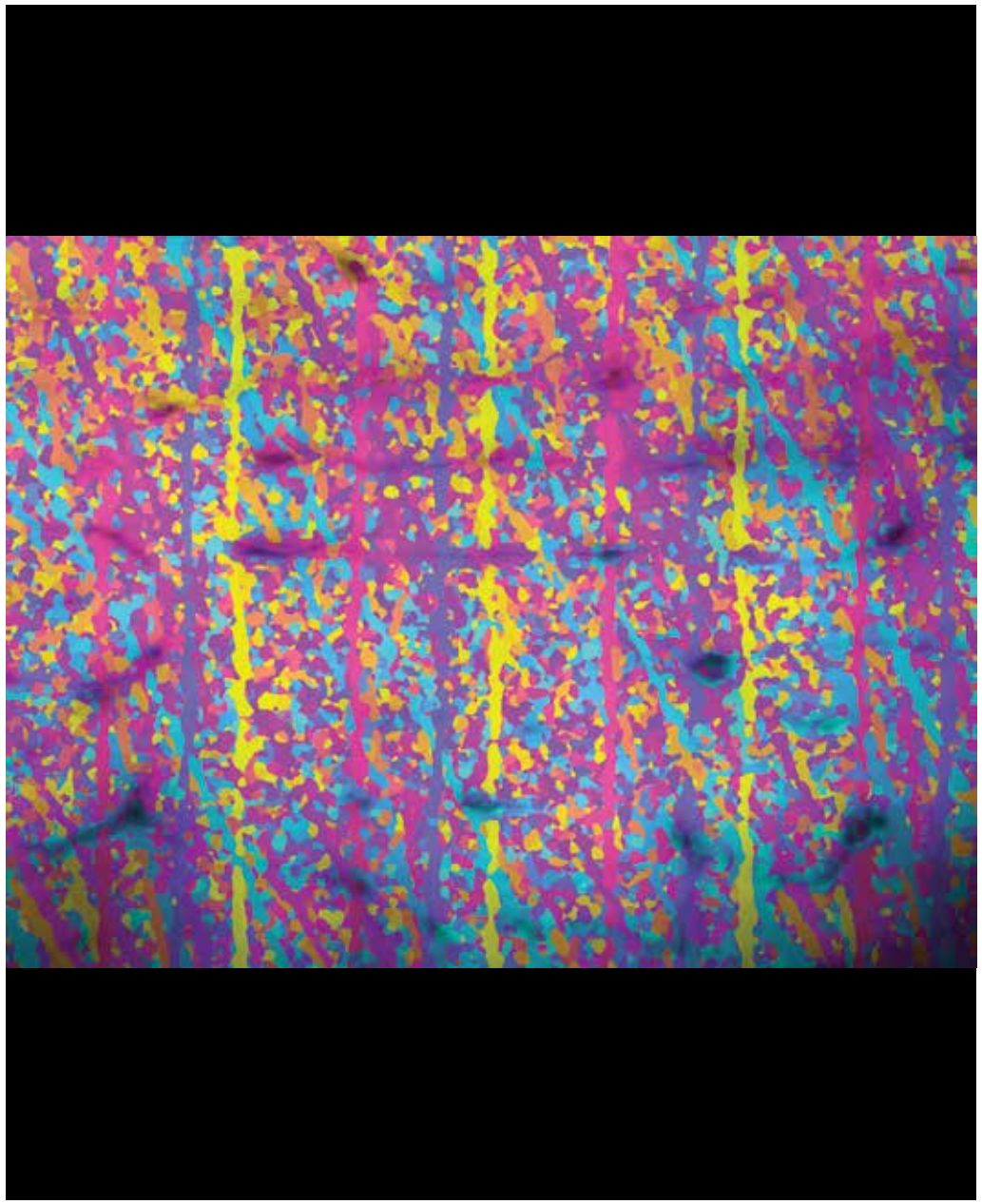

Figure 12. Emu bone tissue image combining microanatomy and preparation artefact. Field width 1.75 mm.

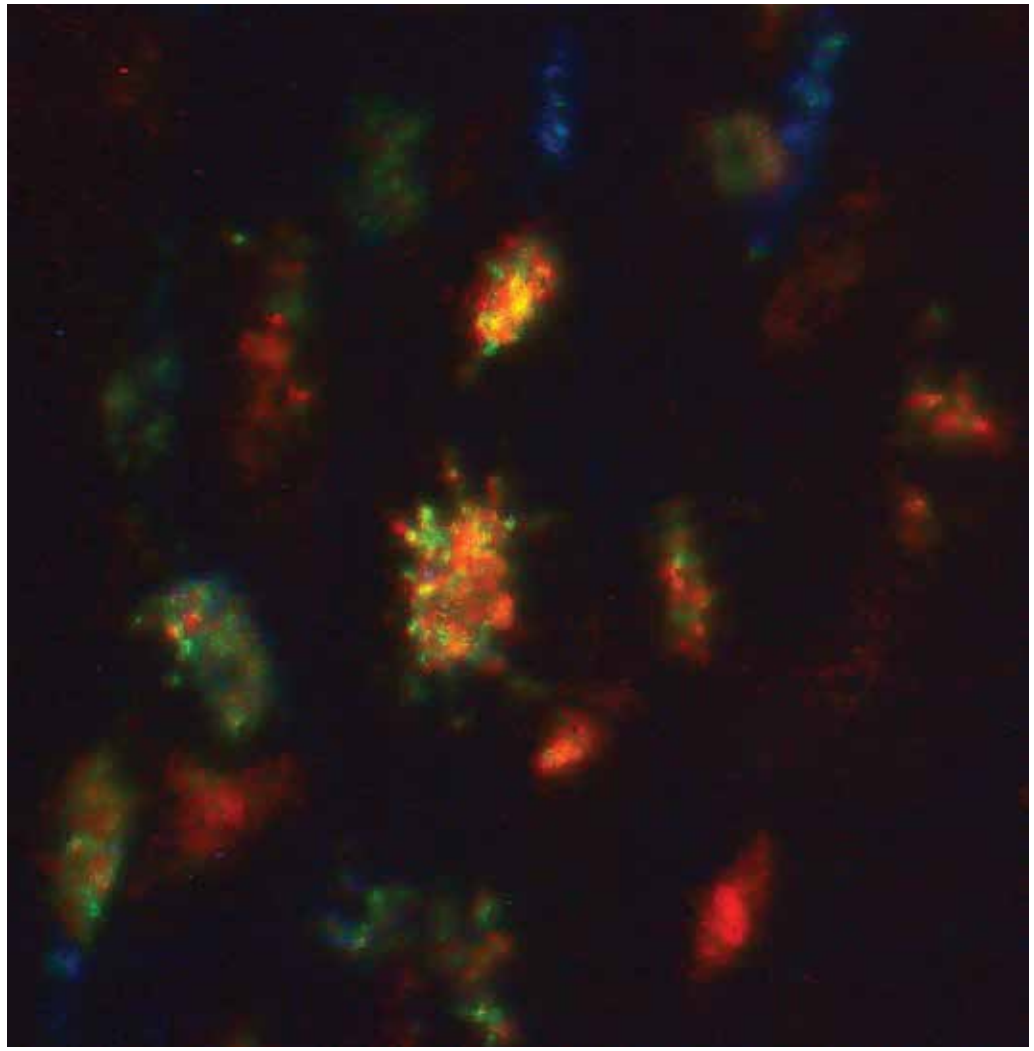

Figure 13. Lucy's bone cell spaces by PCSOM. Field width 110 µm.

Lucy Osteocyte Lacunae

Figure 13 shows a through series of images brought into an all-in-focus image of femoral bone cell spaces called osteocyte lacunae was acquired by PCSOM of the famous "Lucy" skeleton, discovered from fossil bearing deposits at Hadar, Ethiopia, approximately 3 million years old. Polarisation colours are derived from the mineral precipitates inside each lacunae. This image provides information about the degree of orientation of the cell spaces beneath the surface of the bone, which in turn tells us about the way in which the bone was growing during childhood. These well-oriented cells show that the surface was depositing bone during growth, (randomly oriented cells would have meant that the surface was resorbing bone during growth). In addition, because the depth to which the through series is known, we have a defined volume for counting the number of lacunae and comparing this to other primates. The number of lacunae per unit volume is linearly related to growth rate and body size, and Lucy's number agrees closely with that of the Chimpanzee (Bromage et al., 2009b).

Lucy fibre orientation

The image in figure 14 is of femoral collagen fibre orientation (acquired by PCSOM) of the famous "Lucy" skeleton. The circularly polarised light image provides information about the degree of orientation of the collagen fibres within the bone, which in turn can tell us about the ability of the tissue to resist different kinds of mechanical stresses encountered in everyday life; green is collagen perpendicular to the plane of the image, and light blue represents collagen parallel with the image plane. The circular arrangements in the image represent internal remodelling of the bone cortex, in which bone removing cells fashioned a void, which was subsequently filled in by bone forming cells around a central vascular canal. Comparing the organisation of bone tissue between Lucy, belonging to the species *Australopithecus afarensis*, and other species of early human, can help us to understand more about how bone structure and function has varied over human evolutionary time (Bromage et al., 2009a).

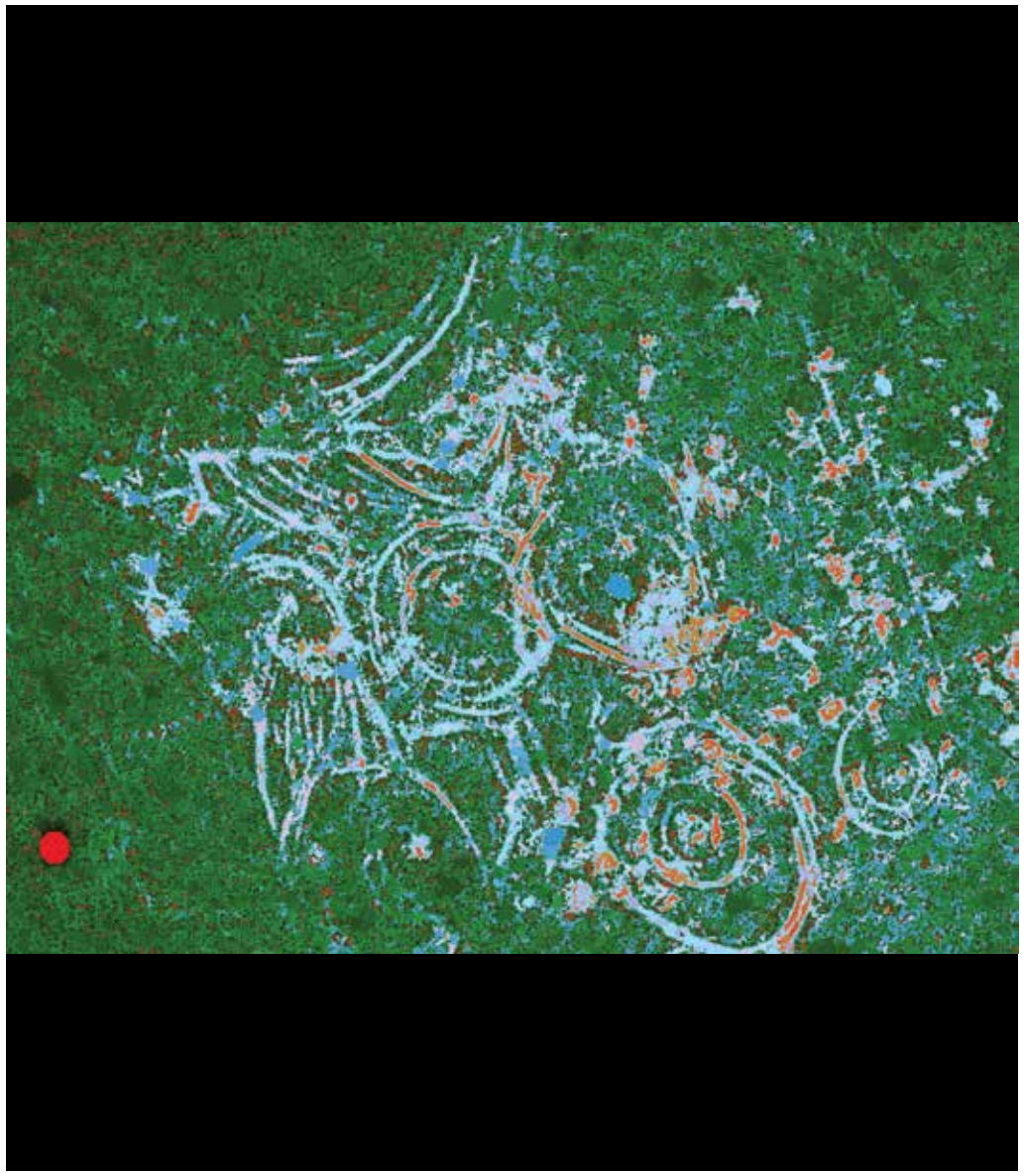

Figure 14. Lucy's collagen fibre orientation by PCSOM. Original size 600 µm.

Rat in space

Figures 15 - 17 show the forelimb bone of a growing rat (*Rattus rattus*) that has flown aboard the NASA Space Shuttle. Each lineation from the bottom to top of the image represents a daily increment of bone growth. Measurement of the widths between increments helped to describe how rat development was affected by zero gravity. Our research shows that bone growth is significantly compromised in space (Bromage et al., 1998). This Space Shuttle research is necessary for appreciating issues related to astronaut health in space and, ultimately, the NASA mission to colonise space, which would include communities complete with growing children.

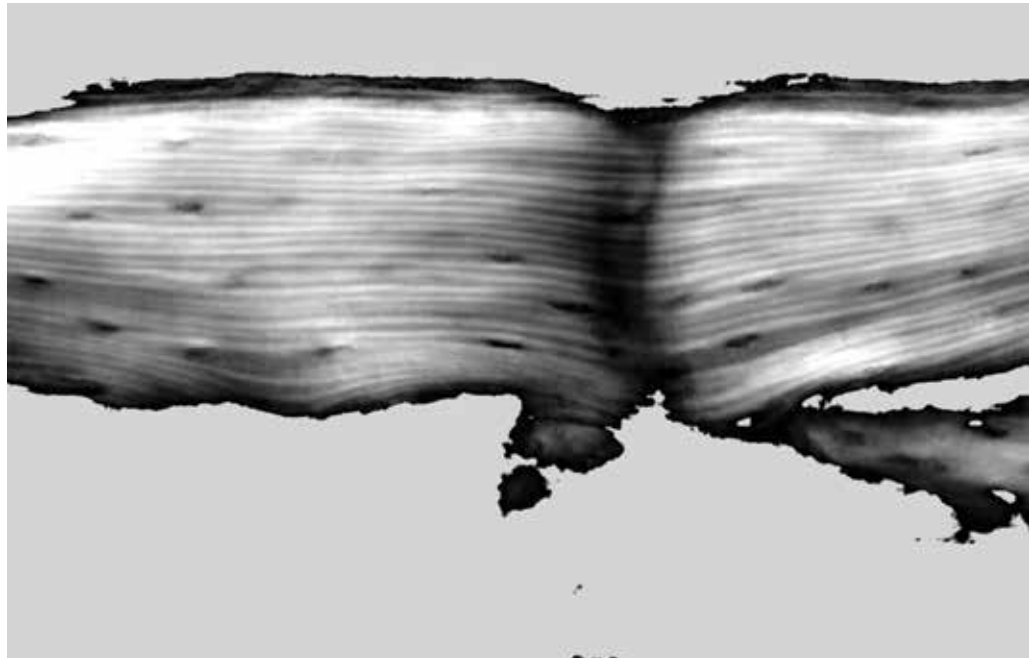

Figure 15. A 100-micron thick section of the bone was imaged in circularly polarised light. Field width 270 µm.

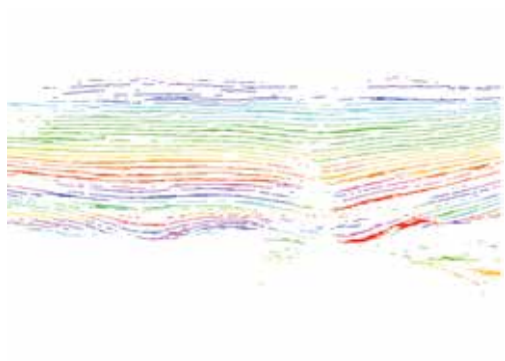

Figure 16. The polarised image was digitally processed to preferentially reveal the binary linear detail (left to right). Field width 270 µm.

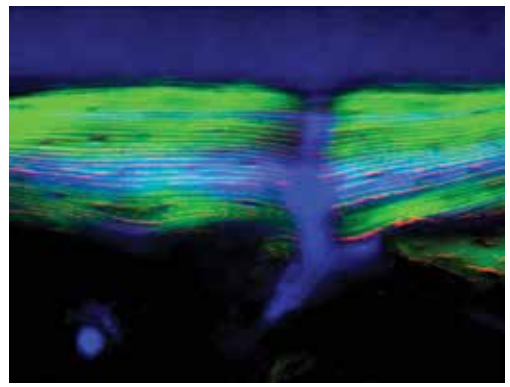

Figure 17. The section was imaged in ultraviolet light to reveal fluorescent markers (blue) given to the rat before and after the Space Shuttle mission. Added to this image were the polarised light and binary images to make a composite for study. Field width 270 µm.

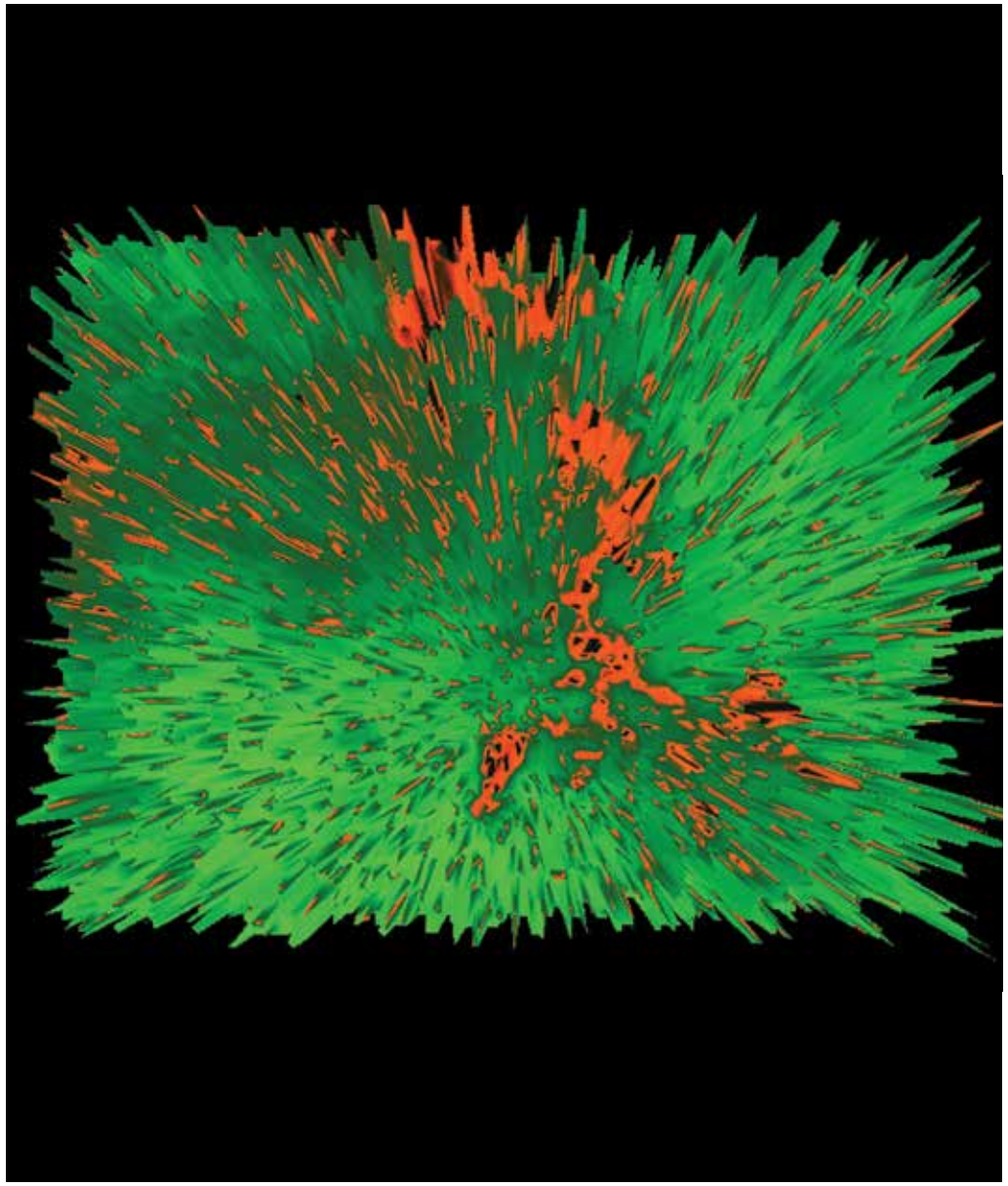

Figure 18. Bacterial tunnelling in facial bone from the "Taung Child" skull. Field width 74 µm.

Taung attack

Figure 18 is a through series of images brought into an all-in-focus image by PCSOM. It reveals bacterial tunnelling in facial bone from the famous "Taung Child" skull discovered from fossil bearing deposits at Taung, Boputhatswana, South Africa, approximately 3 million years old. This image illustrates the nature in which bacterial attack has removed tunnels of bone beneath the surface. The image was acquired by using the autofluorescence potential of bone collagen. Thus, instead of using normal white light, the microscope was configured to image the green coloured fluorescence of bone when using ultraviolet light. The image obtained here is a 3D image of a bacterial attack, the orange colour depicting damage at depth, surrounded by intact bone that is coloured green. By using diffraction grating glasses it can be observed in 3D.

Dental tissues

Zebra dentine

The upper molar dentine of a South African zebra (*Equus burchelli*) is observed by BSE-SEM in Figure 19. The image derives from the polished cut surface of a tooth sectioned through its centre, in which false colours were assigned to levels of grey in the original image. It is called a "density-dependent" image; black represents holes, which are tubes cut in cross section (i.e. no mineralised dentine), blue is least densely mineralised (i.e. relatively less hard dentine), and yellow is most densely mineralised (i.e. relatively more hard peritubular dentine). Each tube was associated with one long dentine cell process in life. The number of holes and the proportion of yellow to blue may characterise certain species and relate to their feeding habits.

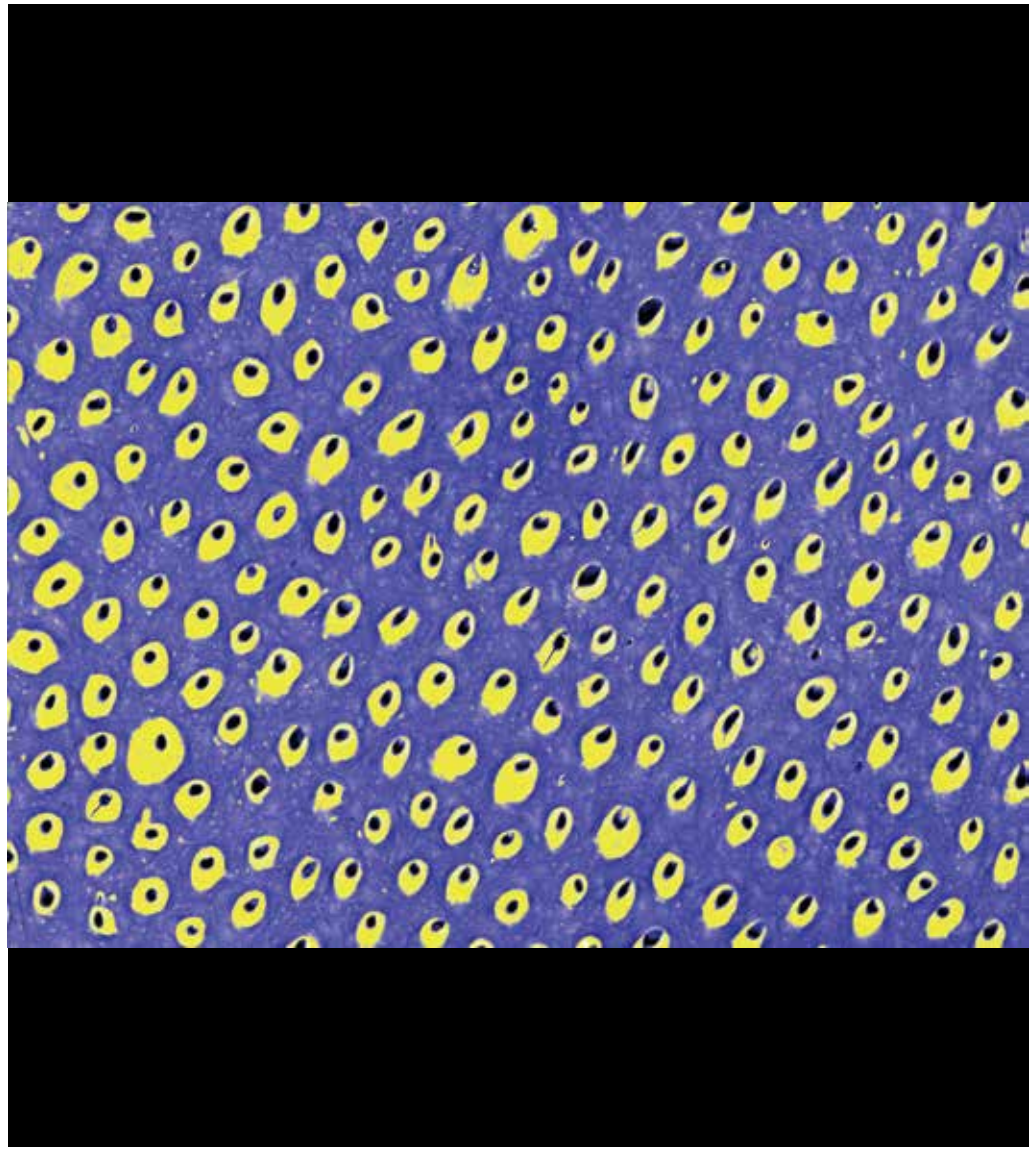

Figure 19. Zebra dentine by BSE-SEM. Field width 265 µm.

Early *Homo*

We imaged enamel macro- and microanatomy of an early human tooth discovered from fossil bearing deposits on the eastern shore of Lake Turkana, Kenya, by PCSOM (Figure 20). Enamel surface macro-anatomy is characterised by vertical bands representing near 7-8 day increments of enamel deposition, called perikymata. Subsurface microanatomical details of enamel prisms are visible as a regular arrangement of small circular spots. False colour is imparted to the grey-level image based on reflection intensities. The deep blue colour at bottom left is sediment adhering to the surface of the tooth.

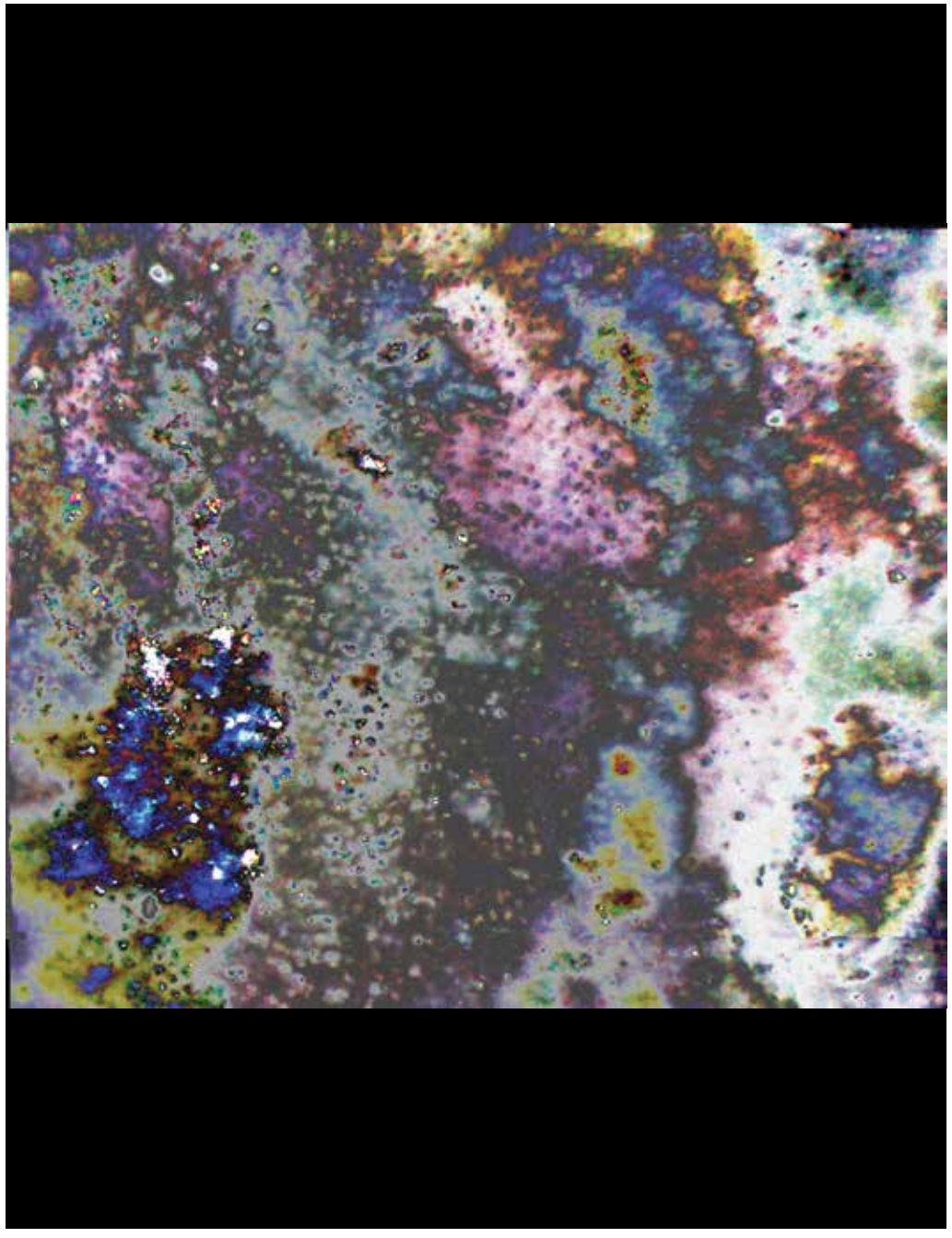

Figure 20. Enamel surface and below surface imaging of a 1.5 million year old early Homo tooth. Field width 600 µm.

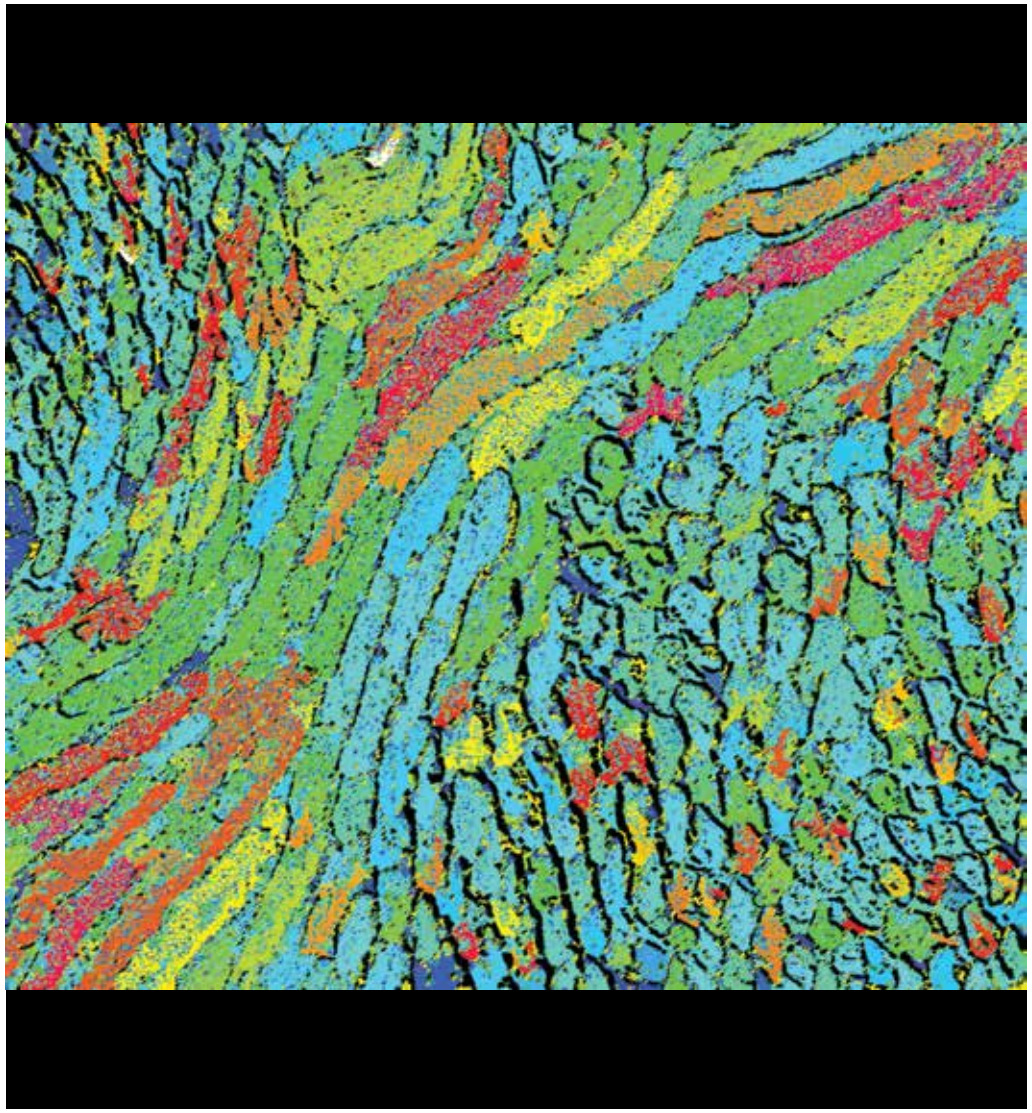

Figure 21. Enamel prism outlines deep in the tooth near the junction with underlying dentine. Field width 180 µm.

Human enamel structure

The enamel of modern humans and their ancestors varies in microanatomical structure in ways that resist the propagation of cracks. To examine this problem it is necessary to image and observe the orientations of units of enamel structure called prisms that course outward from the junction with underlying dentine to the outer surface of the tooth. In this example, modern human enamel deep to the surface of a cut and polished tooth is imaged by backscattered electron imaging in the scanning electron microscope, we see that the prisms have divergent courses (Figure 21). Some prisms are seen to course longitudinally and wander lengthwise in the plane of the image while others course in and out of the plane of the image and appear semi-circular. This heterogeneity provides crack propagating resistance to a tooth, enabling it to withstand the mechanical forces of chewing. Some early hominins with large robust teeth have more anti-crack propagating heterogeneous enamel than other species. Colour was imparted to the image by an algorithm for discriminating enamel prism aspect ratios.

Indented dentine

To determine the strength of a material, such as this polished human dentine slab obtained from a molar tooth, a tetrahedron diamond point is applied to the surface with a known force. Measurements of the indent provide data on the resistance of the tissue to the force. This image was acquired using circular differential interference contrast (Figure 22). Around and within the indent are small round ca. 2 µm diameter tubules that contain the dentine cell processes.

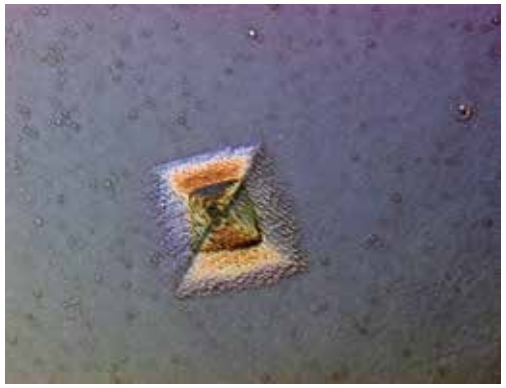

Figure 22. Mechanical testing of human dentine using an indenter. Field width 600 µm.

Cuspal enamel-dentine junction

The cusp of a modern human molar tooth is a wonderfully complex structure (Figure 23). While the mechanisms remain obscure, we can observe the behaviour of enamel forming cells by examining the tooth material they lay down during development. In this histological thin section, the "hill" below, is the dentine of the tooth. From the surface of the dentine, enamel developed upward in swirling patterns that have some relevance to the biomechanical resistance of the tooth to chewing forces. This junction between enamel and dentine is known as the enamel-dentine junction, or EDJ. At tooth cusp tips this swirling phenomenon renders a tissue called "gnarled enamel" for its appearance. Other characteristics observed in this image are "enamel tufts", which are enamel deficient defects arising from the EDJ upward into enamel, here they appear like flames on the surface of dentine. The colour in this image is obtained by using partially circularly polarised light in a conventional compound light microscope. Typically, apart from their general growth trajectory away from the EDJ at cusp tips, because the enamel cells regularly swirl into and out of the plane of section, the enamel is formed in patterns that, when mineralised, reveal crystal orientations which appear in orange when in the plane of the section, or blue when passing up and down through the section.

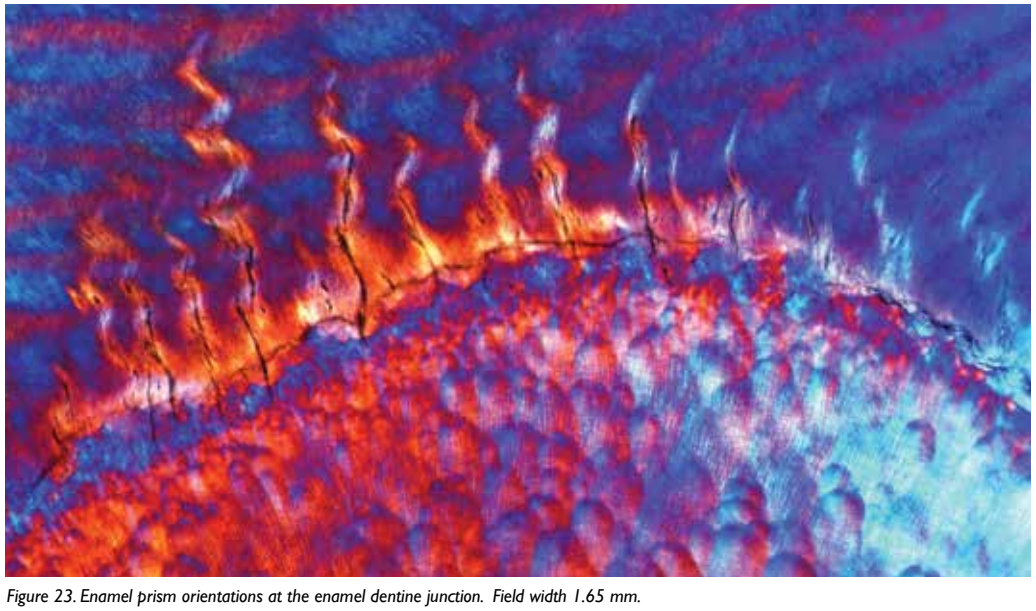

Figure 23. Enamel prism orientations at the enamel dentine junction. Field width 1.65 mm.

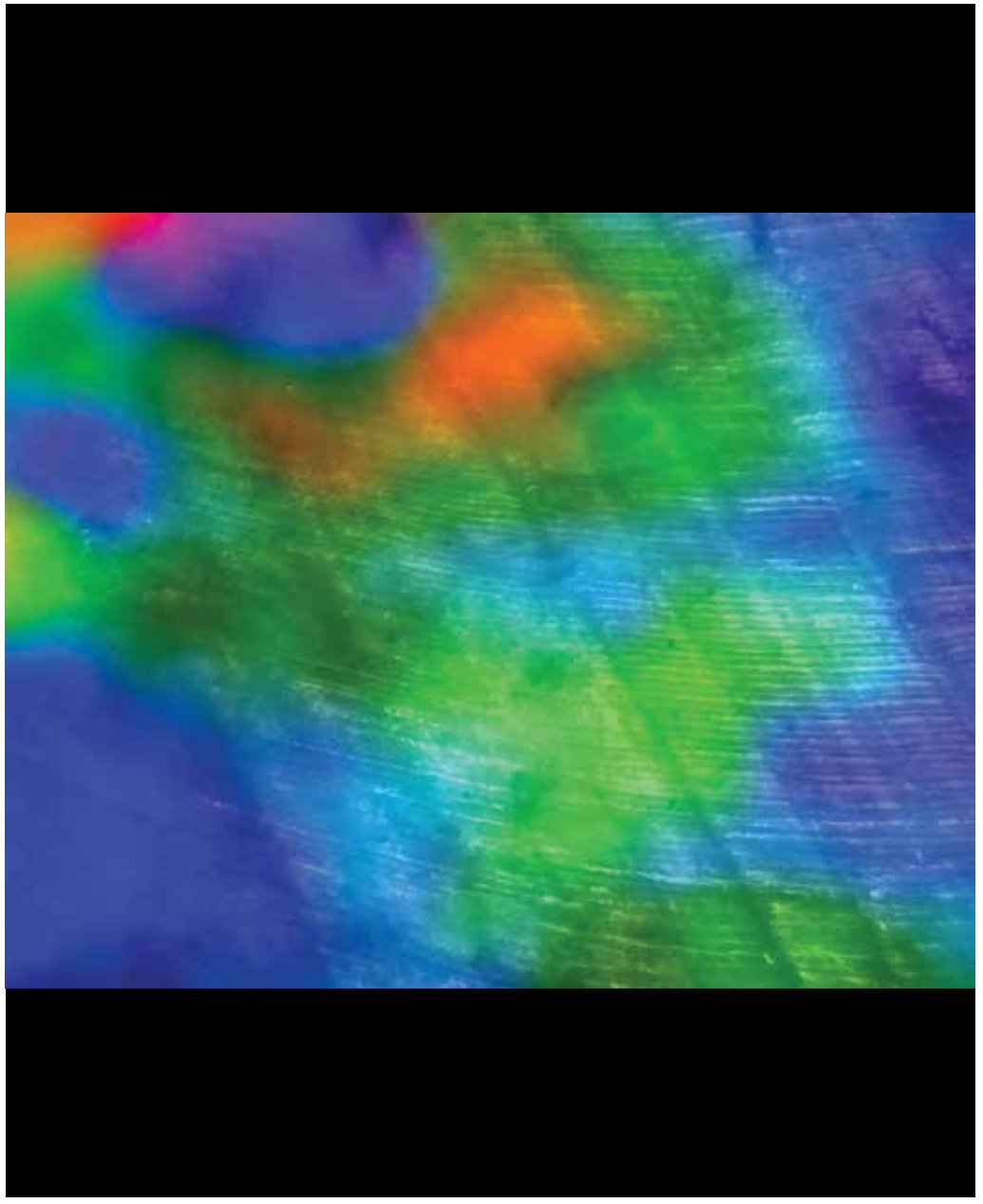

Figure 24. Enamel organisation of Paranthropus robustus by PCSOM. Field width 450 µm.

Paranthropus enamel

Figure 24 shows a through focus series of images brought into an all-in-focus image of the naturally fractured enamel of an early hominin *Paranthropus robustus* molar from Swartkrans, South Africa, ca 2 million years ago. Imaging deep to the enamel surface showed the incremental enamel microanatomy, the striae of Retzius seen from upper left to lower right, across which course the enamel prisms. The striae represent successive forming fronts of the enamel at 7-day intervals. Overlain on this image is a colour relief map of the actual 3D topography of this surface, which varied considerably; orange areas are high and green to blue regions are successively deeper.

Technical applications to bone and dental tissue imaging

Surface staining

Figure 25 (top) shows bovine bone stained with Toluidine blue after using an etching with periodic acid. Figure 25 (bottom) shows a glycoproteic component in enamel prisms of human tooth stained with silver nitrate after etching with periodic acid. In both cases the section was thick (e.g., > 100 µm) but only the surface was stained and observed in bright-field microscopy using diffusing light.

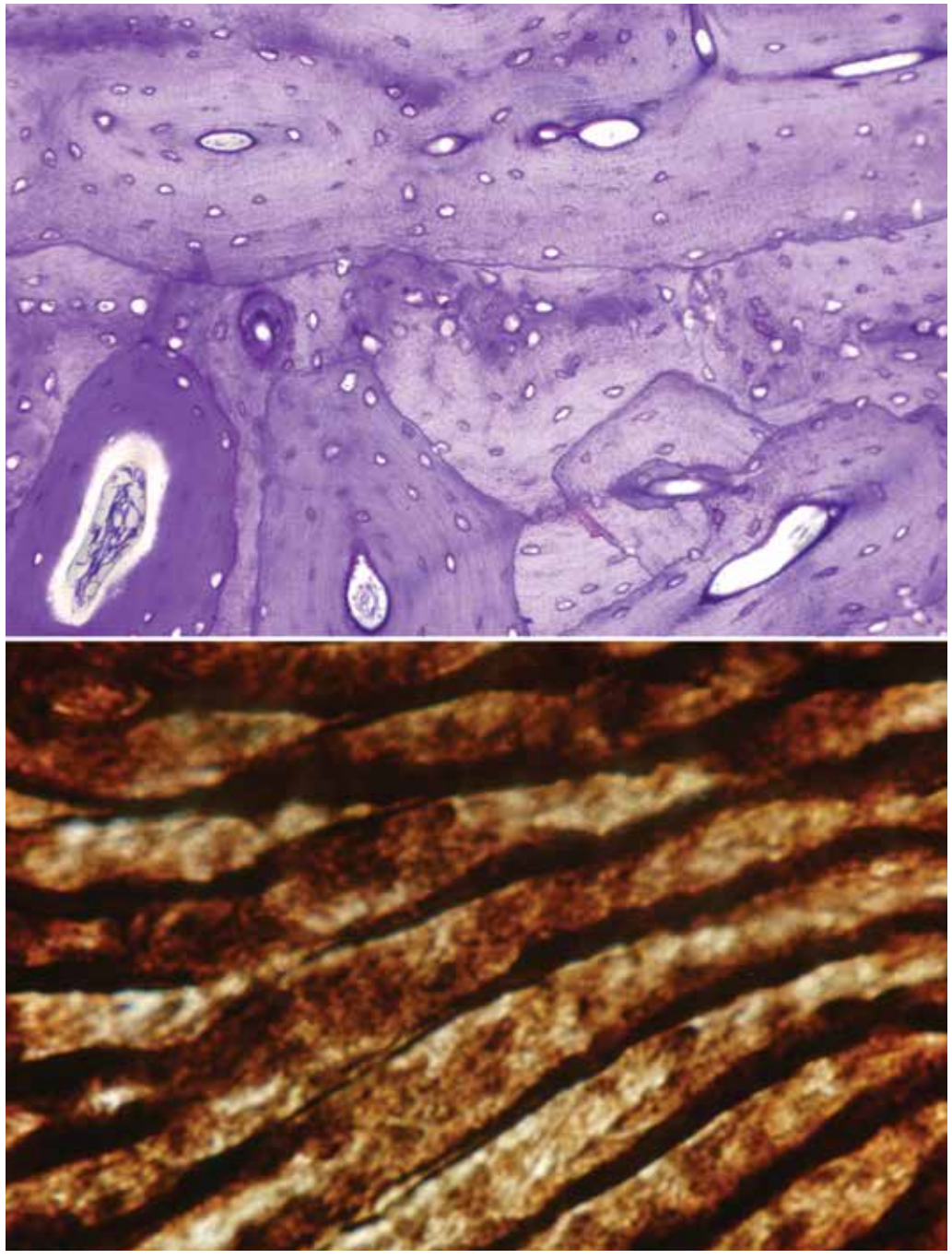

Figure 25. Bone (top) and enamel (bottom) surface staining. Field widths 655 µm (top) and 65 µm (bottom).

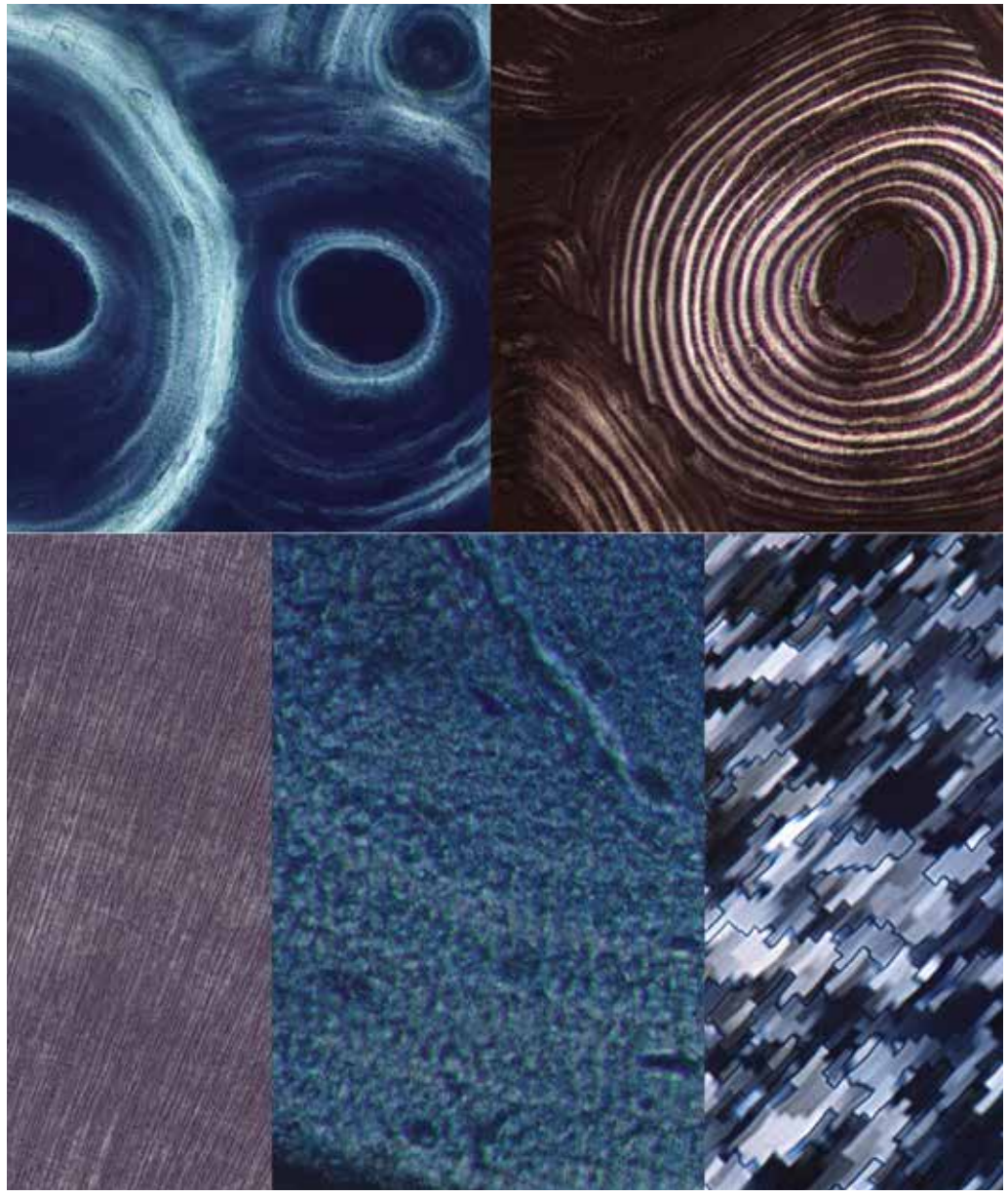

Figure 26. Hard tissues imaged by polarised light microscopy (see text for details). Field widths: top, = 315 µm each; bottom, 420 µm (left), 81 µm (centre), 42 µm (right).

Ordinary Polarisation

Figure 26 shows examples of polarisation. Top, left - Decalcified human remodelling units (osteons) observed with circularly polarised light. Top, right - Human osteons from a slice of human femur bone that has previously been heated to 220°C for 1 day in order to remove the organic material-observed with circularly polarised light. Bottom, left - Dentine of a killer whale tooth observed with crossed-polarisation. Bottom, centre - Detail of an osteon from a fossil dinosaur bone (*Spinosaurus*) observed with crossed-polarisation. Bottom, right - Mother-of-pearl observed with crossed-polarisation. The contribution to the polarisation image of the mineral predominates and gives grey (and white) in all but the first image (which was decalcified).

Optimising images with a compensator

Figure 27 (left) shows a *Mosasaurus* tooth observed with crossed-polarisation. Only the enamel is visible while the dentine is not as it gives almost black. The right image shows the same tooth observed by inserting 1/4 lambda compensator. Dentin is now visible in shades of grey. The dentine shows two lines of growth arrest whose separation could correspond to a year in the life of the animal.

Figure 27. Polarised light microscopy of dental tissues combined with a compensator to enhance orientation-dependent contrast. Field widths 1.64 mm (left) and 524 µm (right).

Optimising images with dichroic mirrors

Figure 28 (left column) shows two Borax particles that have been oriented so that one gives interference colours, and the other gives almost black when viewed with cross-polarisation. However the particle on the right is visible when using dichroic mirrors. These mirrors introduce 1/4 lambda retardation. Note that the background also changes from black to a blue or green colour depending on the mirror used. The right column of figure 28 shows: top - A chick tibiotarso bone seen in a longitudinal section using a "blue" dichroic mirror. Bottom - Primary bovine bone osteons observed in a longitudinal section using a "green" dichroic mirror.

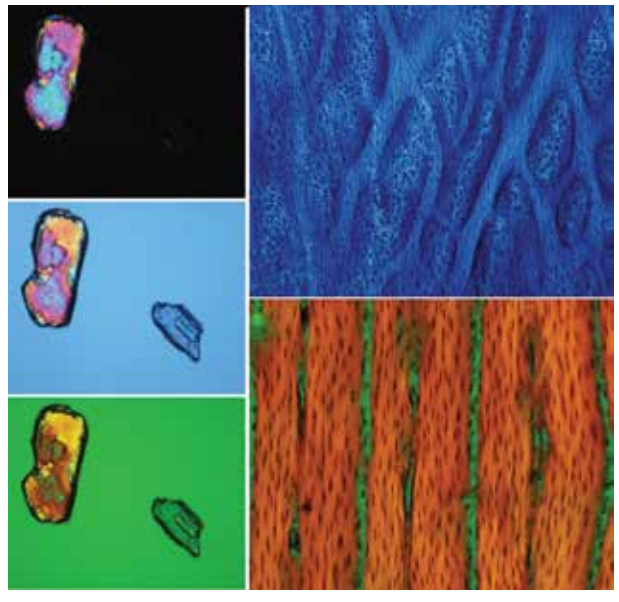

Figure 28. Polarised light microscopy of bone tissues combined with a dichroic mirror to enhance contrast. Field widths 655 µm (all images).

Monochromatic Polarisation

Figure 29 shows the detail of the organisation of the collagen fibres in a secondary osteon from a human femur. The section is very thin (less than 15 um) and has been decalcified and stained with Phosphomolybdic acid. To obtain a monochromatic polarisation image, a 1/4 lambda retarder and a 546nm band pass filter are inserted in the optical path, always before the analyser. This configuration is similar to that used with the Senarmont compensator.

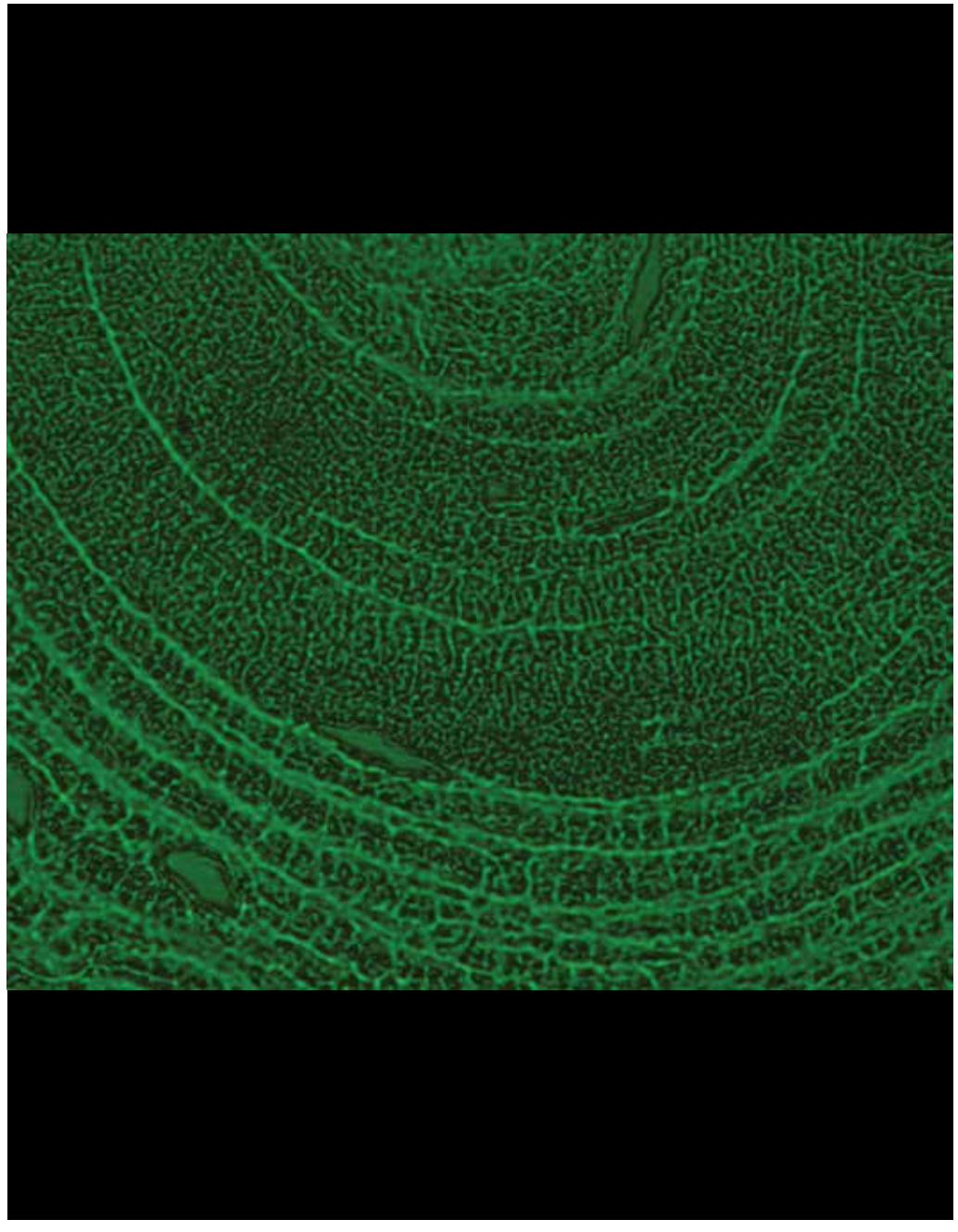

Figure 29. Decalcified bone section imaged by monochromatic polarisation. Field width = 127 µm.

Fish scale

Fish in space

Figure 30 shows the scale of a Zebra fish (*Xiphophorus helleri*) which was flown aboard the NASA Space Shuttle. Fish scales grow from the small inner ring outward, the number of rings corresponds to the age of the fish. This image was acquired with partially polarised light combined from transmission and incident light sources using a stereo zoom microscope. Measurement of the width between rings help to describe how the fish reacts to zero gravity. Preliminary studies indicate that growth rate is little perturbed, establishing the future possibility of developing aquaculture in space.

Figure 30. Scale from a fish flown aboard the Space Shuttle. Field width 2 mm.

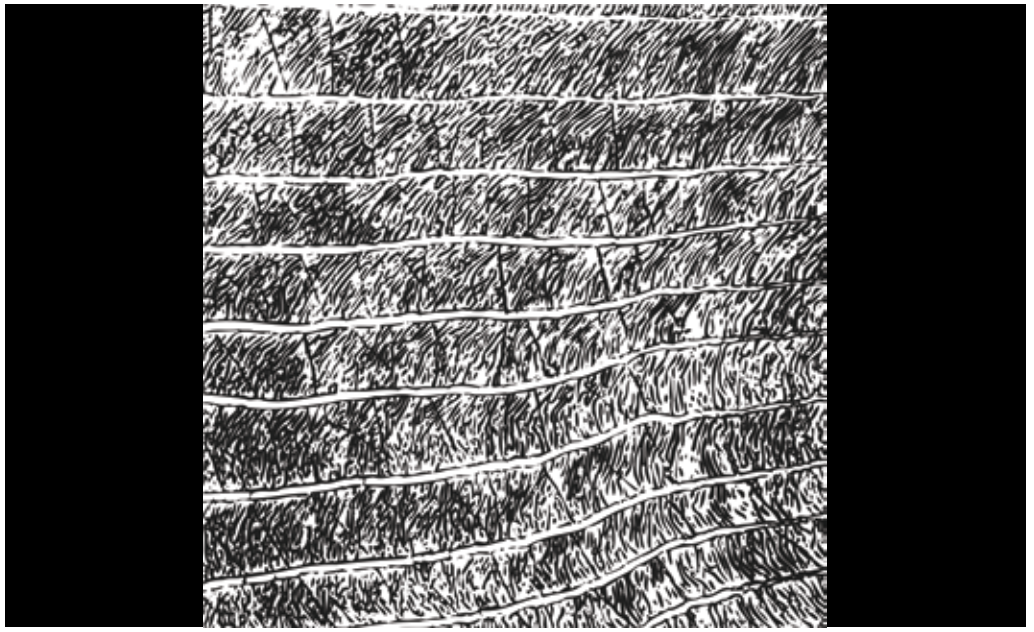

Figure 31. Scale from fish living in a lake distant from the Chernobyl nuclear power plant. Field width 250 µm.

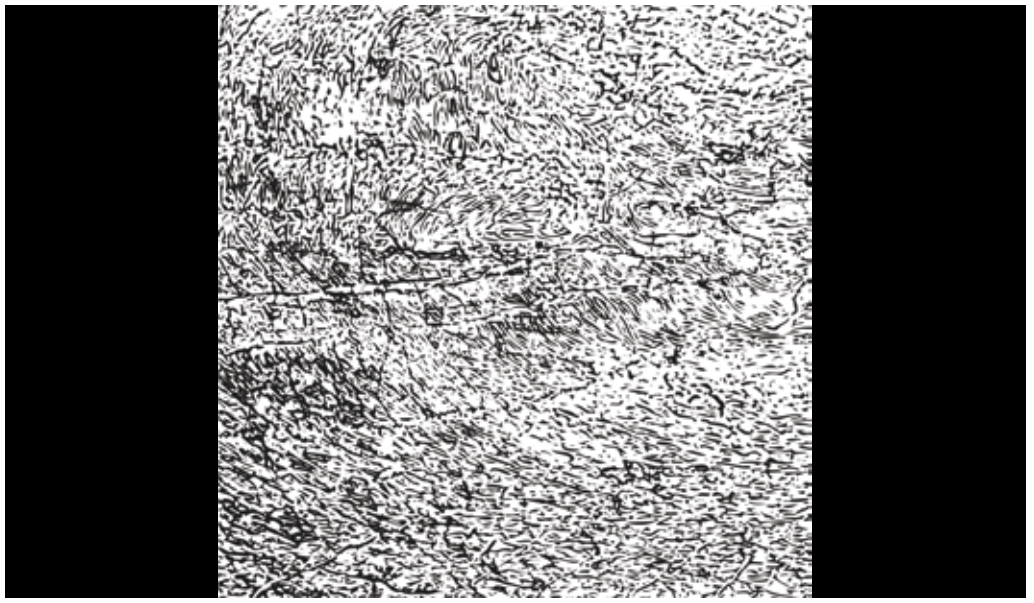

Figure 32. Scale from fish living in lake near to the Chernobyl nuclear power plant. Field width 250 µm.

Chernobyl

Figure 31 was acquired with conventional transmission compound microscopy. The rings, called circuli, of a fish scale represent increments of growth; their departure from uniform widths between rings is an indication of variation in growth rate. Thus waters that are polluted, too warm, or too cold, affect the growth rate of the fish and its scales. We notice that the rings of Tench (*Tinca tinca*) living near to the Chernobyl nuclear power plant following the April 26, 1986 disaster (Figure 32). are of a different character than those of fish living in lakes far away from the plant.

Acknowledgments

We are grateful to the curators and staff of the following for their permissions to study early hominin material in their care: Ethiopia National Museum, Addis Ababa, Ethiopia; National Museums of Kenya, Nairobi, Kenya; Transvaal Museum, Pretoria, South Africa; Universidad Complutense de Madrid; University of the Witwatersrand Medical School, South Africa.

Biographies

Tim Bromage, PhD

Tim Bromage is Professor of Biomaterials and Biomimetics at New York University's College of Dentistry. His principal interests include using hard tissue biology to address questions relating to the life histories of mammals and to understand connections between the environment and bone and tooth microanatomy.

Santiago Gomez MD PhD MRCPath

Santiago Gomez is Professor of Pathology at the Faculty of Medicine, University of Cadiz, Spain. Although he defines himself as a microscopist, he enjoys preparing thin sections himself, using either the knife, sandpaper, and polishing cloths. He is passionate about hard tissues and searching for the recording structures they contain.

Alan Boyde, PhD, BDS, LDSRCS, MDhc, FRMS, FAS

Alan Boyde is Professor of Mineralized Tissue Biology at Queen Mary University of London. His research interests are in dental and skeletal hard tissue development, structure, function, disease and treatment. Skeletal tissue responses to hormonal and drug challenges, impact exercise, aging, osteomalacia, osteoporosis, osteoarthritis, traumatic osteochondrosis, fatigue fracture, dental and skeletal implants, tumour metastases. Skeletal changes in genetically modified mice.

References

Boyde, A., Bianco, P., Portigliatti Barbos, M., Ascenzi, A. (1984) Collagen orientation in compact bone: I. A new method for the determination of the proportion of collagen parallel to the plane of compact bone sections. Metab Bone Dis Relat Res 5:299–307.

Boyde, A., Mccorkell, F.A., Taylor, G.K., Bomphrey, R.J., Doube, M. (2014) Iodine vapor staining for atomic number contrast in backscattered electron and x-ray imaging. Microscopy Research and Technique 77: 1044-1051.

Boyde, A. (1995) Confocal optical microscopy. In: Image Analysis in Histology: Conventional and Confocal Microscopy, Eds: Wootton, R., Springall, D.R. and Polak, J.M. Cambridge University Press, Cambridge, UK, pp 151-196.

Boyde, A., Petran, M., Hadravsky, M. (1983) Tandem scanning reflected light microscopy of internal features in whole bone and tooth samples. Journal of Microscopy 132:1-7.

Bromage, T.G., Boyde, A., Perez-Ochoa, A. (2003a) The Portable confocal microscope: Scanning optical microscopy anywhere. In (Méndez-Vilas A, Ed) Science, Technology and Education of Microscopy: An Overview. Formatex: Badajoz. pp. 742-752.

Bromage, T.G., Goldman, H.M., McFarlin, S., Warshaw, J., Boyde, A., Riggs, C. (2003b) Circularly polarised light standards for investigations of collagen fiber orientation in bone. Anatomical Record: The New Anatomist 274B: 157–168.

Bromage, T.G., Goldman, H.M., McFarlin, S.C., Perez-Ochoa, A., Boyde, A. (2009a) Confocal Scanning Optical Microscopy of a 3my *Australopithecus afarensis* Femur. Scanning 31: 1-10.

Bromage, T.G., Lacruz, R.S., Hogg, R., Goldman, H.M., McFarlin, S.C., Warshaw, J., Dirks, W., Perez-Ochoa, A., Smolyar, I., Enlow, D.H., Boyde, A. (2009b) Lamellar bone is an incremental tissue reconciling enamel rhythms, body size, and organismal life history. Calcified Tissue International 84: 388-404.

Bromage, T.G., Smolyar, I., Doty, S.B., Holton, E., Zuyev, .AN. (1998) Bone growth rate and relative mineralisation density during space flight. Scanning 20: 238-239.

Bromage, T.G. (1987). The SEM/replica technique and recent applications to the study of fossil bone. Scanning Electron Microscopy 1987: 607-613.

Greenberg, G.L. & Boyde, A. (1997) Convenient and controllable direct-view 3D imaging in conventional optical microscopes: approaches via illumination and inspection. Proc Roy Microsc Soc 32:87–100.

Greenberg, G.L. & Boyde, A. (1997) Convenient and controllable direct-view 3D imaging in conventional light microscopes: approaches via illumination and inspection. Proc Roy Microsc Soc. *32*, 87-100.

Kino, G.S. (1995) Intermediate optics in Nipkow disk microscopes. In: Handbook of Biological Confocal Microscopy, Ed: Pawley, J.B. Plenum Press: New York. pp155-165.

Petran, M. & Hadravsky, M. (1966) Method and arrangement for improving the resolving power and contrast. US Patent No. 3,517,980, priority 05.12.1966, patented 30.06.1970 US.

Yeh, N., Miller, J.P., Gaur, T., Capellini, T.D., Nikolich-Zugich, J., la Hoz, C. de, Selleri, L., Bromage, T.G., van Wijnen, A.J., Stein, G.S., Lian, J.B., Vidal, A., Koff, A. (2007) Cooperation between p27 and p107 during endochondral ossification suggests a genetic pathway controlled by p27 and p130. Molecular and Cellular Biology 27: 5161-5171.